Metals and Materials International
https://doi.org/10.1007/s12540-018-0079-6

Microstructural and Textural Differences Induced by Water and Furnace Cooling in Commercially Pure Zr Annealed in the α + β Region

Linjiang Chai[1] · Tingting Wang[1] · Yi Ren[2] · Bo Song[3] · Ning Guo[3] · Liangyu Chen[4]

Received: 19 September 2017 / Accepted: 3 December 2017

Abstract
In this work, a commercially pure Zr sheet with a typical bimodal basal texture was annealed in an α + β region and then subjected to different coolings (in water and furnace). Microstructures and textures of both the as-received and the heat-treated specimens were investigated by electron channeling contrast imaging and electron backscatter diffraction techniques. Results show that a duplex microstructure consisting of untransformed bulk α grains and twinned martensitic plates is produced in the water-cooled specimen, which possesses a weakened texture compared to the initial one. For the specimen cooled in furnace, however, a uniform microstructure fully comprised of coarser equiaxed grains with a strengthened texture is obtained. Analyses reveal that the rapid cooling in water could suppress variant selection behaviors during β → α transformation and allow α plates with scattered orientations to be nucleated inside β phases, contributing to the weakened texture. In contrast, during slow cooling in furnace, β boundaries would act as preferred nucleation sites of α embryos, resulting in a strong variant selection that accounts for the intensified texture.

Keywords Zirconium · Microstructure · Texture · Phase transformation · Cooling rate

1 Introduction

Owing to attractive corrosion and irradiation resistance, Zirconium (Zr) and Zr alloys are nowadays widely used in chemical and nuclear industries [1–5]. At room temperature, these Zr materials essentially have a hexagonal close packed (hcp) structure (α phase), which will be allotropically transformed into a body centered cubic (bcc) structure (β phase) at elevated temperatures. Typically, fabrication processes of the Zr base products (like tubes and sheets) are carried out below the α/β transformation temperature. Since a limited number of slip systems can be offered by the hcp α-Zr, strong crystallographic textures are usually developed after such fabrications [6–8]. As a result, undesirable anisotropy in elasticity modulus, irradiation growth, creep, plasticity and fracture toughness is often noted for Zr and Zr alloys [6, 9, 10].

In earlier work, some efforts were attempted to alter the easily developed textures by resorting to phase transformation heat treatments [11–14]. It is well-known that the hcp α-Zr and the bcc β-Zr can be related by the Burgers orientation relationship (OR) [15]: $\{0001\}_\alpha // \{110\}_\beta$ and $<11\text{-}20>_\alpha // <111>_\beta$. According to this OR, one β orientation could give birth to twelve equivalent α-orientation variants during β → α cooling. The presence of all these variants will allow an initial texture to be considerably randomized. However, some researchers noted that strong variant selection (only a limited number of variants appear) often occurred so that the obtained transformation texture was similar to or even stronger than the initial one [11–13, 16, 17]. Such

✉ Linjiang Chai
chailinjiang@cqut.edu.cn

✉ Liangyu Chen
lychen@just.edu.cn

1 College of Materials Science and Engineering, Chongqing University of Technology, Chongqing 400054, China

2 School of Mechanotronics and Vehicle Engineering, Chongqing Jiaotong University, Chongqing 400074, China

3 Faculty of Materials and Energy, Southwest University, Chongqing 400715, China

4 School of Mathematics and Science, Jiangsu University of Science and Technology, Zhenjiang 212003, Jiangsu, China

Published online: 12 March 2018

texture memory phenomena were reported to be more notable when Zr alloys were heat-treated in α + β regions [11, 12].

Nevertheless, researchers have tried to explore specific factors (like peak temperature [11] and applied stresses [17] during heating) that influence the variant selection. Note that the cooling rate is also an important processing parameter that can be feasibly adjusted in practice, for example using different cooling media. In spite of the long-recognized effect of cooling rates in producing various microstructural features of Zr alloys [18–21], their definite influence on the transformation texture has not been well explored. Therefore, in the present work, a commercially pure Zr (cp-Zr) with a typical texture was heat-treated in an α + β region and then cooled in two different ways (in water and furnace). For these specimens cooled at different rates, their microstructure and orientation features were carefully characterized and compared to clarify the comprehensive effect of cooling rates on the transformation microstructure and texture.

2 Experimental

A recrystallized Zr sheet in commercial purity (1.15 wt% Hf, 0.15 wt% O and < 0.08 wt% Fe + Cr) was selected as the starting (as-received) material. By differential scanning calorimetry, an α + β dual-phase region was determined for the Zr material to exist in the range of ~ 800–1000 °C. Specimens with the dimension of 12 mm × 10 mm × 2 mm were cut from the as-received cp-Zr sheet along rolling, transverse and normal directions (RD, TD and ND), respectively. The specimens were then capsulated in quartz tubes under vacuum and annealed at 900 °C for 30 min in a SX2-8-16 box furnace. After the annealing, they were cooled down to room temperature in two ways, i.e. quenched into cold water or simply left in the power-off furnace. Estimated cooling rates for the water cooling (WC) and the furnace cooling (FC) were ~ 1000 and ~ 0.02 °C/s, respectively [21, 22].

Microstructural and textural characterization of the specimens was mainly performed by an electron backscatter diffraction (EBSD) analysis system in a Zeiss Sigma HD field emission gun scanning electron microscope (FEG-SEM). The EBSD system consisted of an Oxford Instruments NordlysMax^2 detector, with AZtec 2.4 and Channel 5 software packages for data acquisition and post-processing, respectively. The rapid data acquisition promised by the modern EBSD enables both textures and local orientation features to be reliably measured [23, 24]. An electron channeling contrast (ECC) imaging technique based on the FEG-SEM was also utilized for direct microstructural observation. Mechanical grinding and electro-polishing were carried out for specimen RD-ND surfaces before ECC and EBSD examinations, with detailed preparation procedures available elsewhere [25].

3 Results and Discussion

3.1 The As-Received Material

Microstructure and texture of the as-received specimen are presented in Fig. 1. Figure 1a is an ECC image revealing

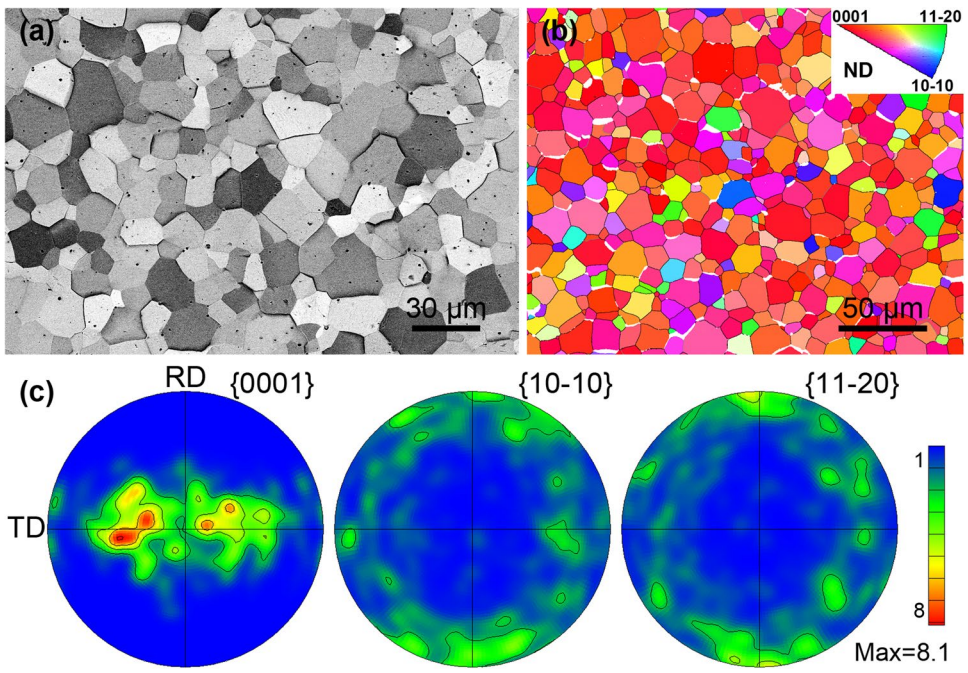

Fig. 1 **a** ECC image, **b** EBSD IPF map and **c** pole figures of the as-received material. In **b**, grain orientations are colored according to the inset while black and gray lines represent HABs and LABs, respectively; **c** corresponding to **b**. (Color figure online)

a rather homogeneous structure, which is comprised of well-equiaxed grains and a few randomly distributed black dots. Composition analyses by energy dispersive spectroscopy suggest these black dots to be second phase particles (SPPs) containing Fe and Cr. Such a microstructure has been frequently observed for Zr alloys after sufficient recrystallization annealing [26–29]. Figure 1b is an EBSD inverse pole figure (IPF) map with high angle boundaries (HABs, $\theta > 15°$) and low angle boundaries (LABs, $2° < \theta \leq 15°$) indicated by black and gray lines, respectively. Most of the boundaries are found to be HABs which should be generated during the prior recrystallization annealing. By the linear intercept method, an average size of grains enclosed by the HABs is measured to be 8.3 ± 5.7 μm. According to the color code (the inset) in Fig. 1b, one can also see that many grains have c-axes aligned towards the ND of the sheet, suggesting preferred grain orientations (crystallographic texture). Pole figures calculated from the EBSD dataset are shown in Fig. 1c to reveal more definite textural features. From the {0001} pole figure, a bimodal basal texture with density maxima (8.1 times random) inclined $\pm \sim 20$–$40°$ from the ND towards the TD is noticeable. In addition, prismatic pole figures show that either <10-–0> or <11–20> direction of most grains is close to the RD. It is to be noted that such a textural feature is very representative in rolled and recrystallized Zr and Zr alloy sheets (e.g. [7, 8]).

3.2 After Annealing in the α + β Region

Microstructural observations (ECC images) of the heat-treated specimens are presented in Fig. 2. After water cooling, the prior homogeneous equiaxed grains seem to be replaced by a duplex microstructure, i.e. coexistence of bulk grains and plate structures (Fig. 2a). As the annealing temperature (900 °C) corresponds to the dual-phase region, the plates and the bulk grains should result from $\beta \rightarrow \alpha$ transformation and untransformed equiaxed grains, respectively. A closer observation in Fig. 2b for the plate structures reveals that most of them have submicron widths with many internal fine twins (nanoscale in lamellar thickness). This suggests that the plate structures should be twinned martensites produced during the $\beta \rightarrow \alpha$ transformation by rapid water cooling [20, 30, 31]. Different from the WC case, duplex microstructures are not seen after furnace cooling. Instead, fully equiaxed grains are found to be the main microstructural characteristic of the FC specimen (Fig. 2c), similar to that observed for the as-received specimen (Fig. 1a). Nevertheless, evident grain growth along with coarsened SPPs can be noticed from Fig. 2d. For these coarse equiaxed grains, some of them grow from prior α grains in the starting material, while others should be transformed from β phases appearing during the annealing in the α + β region. In fact, the shape of α-Zr products generated by β parents would change from plate-like to equiaxed morphology with decreasing cooling rates, as noted for Zircaloy-4 [20]. Anyhow, due to structural homogeneity, it is hard to distinguish the grown and the transformed α grains in the FC specimen.

Figure 3 shows EBSD results revealing quantitative orientation (texture) characteristics of the WC and the FC specimens. According to their IPF maps (Fig. 3a, b), most grains are seen to be colored close to red, similar to the case of the as-received specimen. This suggests essential

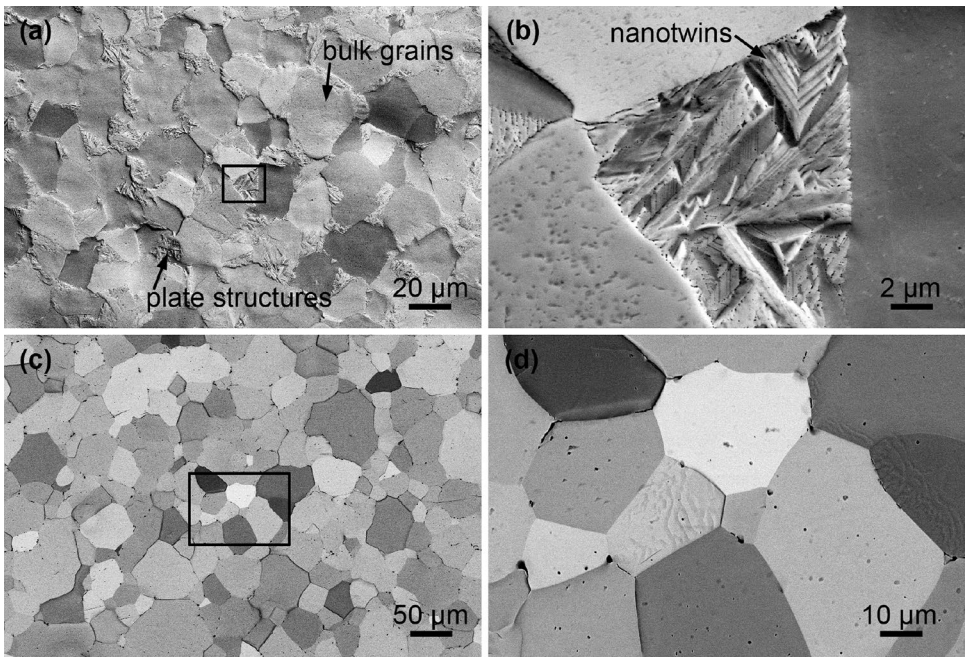

Fig. 2 ECC observations of **a**, **b** the WC and **c**, **d** the FC specimens; **b**, **d** corresponding to boxed regions in **a**, **c**, respectively

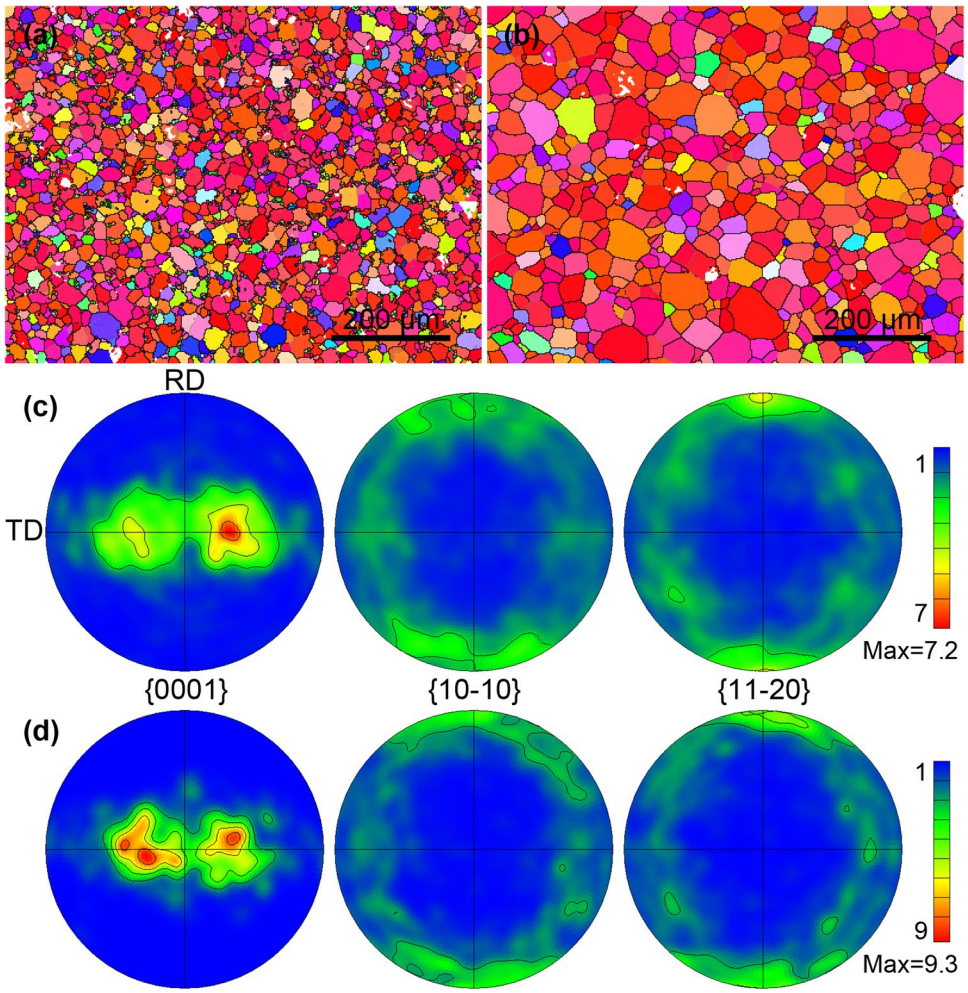

Fig. 3 **a**, **b** EBSD IPF maps (step size 2 μm) of the WC and the FC specimens, respectively; **c**, **d** pole figures corresponding to **a**, **b**, respectively. Color codes for **a**, **b** are the same as that in Fig. 1b. (Color figure online)

inheritance of the original orientation preference after the annealing. In regards to grain morphologies, almost all grains in the FC specimens are confirmed to be equiaxed (Fig. 3b), consistent with the ECC observation (Fig. 2c, d). For the WC specimen, however, although the equiaxed grains can account for the majority of its microstructure, a number of small crystallites (corresponding to plate structures) are also noticeable (Fig. 3a). Since relatively large areas (~ 0.5 mm^2) are covered in Fig. 3a in order to acquire reliable texture information, the step size used here is unavoidably overlarge for examining details of the plate structures.

Pole figures of both the annealed specimens are displayed in Fig. 3c and d. The main features of the prior bimodal basal texture (Fig. 1c) seem to be unchanged after annealing at 900 °C. In fact, the maximum intensity (8.1 times random) of the prior texture is found to be decreased to 7.2 and increased to 9.3 for the WC and the FC specimens, respectively. In other words, the water cooling after annealing in the dual-phase region leads to a weakened texture while textural strengthening occurs upon the furnace cooling.

Since bulk (equiaxed) grains exist in all specimens, their size measurements are also performed by EBSD for the WC and the FC specimens, as shown in Fig. 4. Compared to that (8.3 μm on average) of the as-received specimen, the equiaxed grains in both the heat-treated specimens are markedly larger. For the WC specimen, it is known that after annealing for 30 min α grains will cease to grow during rapid water cooling. Thus, its average size (20.8 μm) should be able to reflect the grain growth limit promised by the heating duration. In contrast, for the FC specimen, the larger average size (30.3 μm) of equiaxed grains indicates that further growth can readily proceed during the much slower cooling.

Since both bulk grains and plate structures of the duplex microstructures in the WC specimen are indexed by EBSD (Fig. 3a), their specific contributions to the global texture are allowed to be probed. As shown in Fig. 5a, b, IPF maps corresponding to the bulk grains and the plate structures are roughly separated, using a grain size of 10 μm as the criterion. Pole figures derived from Fig. 5a and b are presented in Fig. 5c and d, respectively. Figure 5c reveals that the bulk grains in the WC specimen actually own very close

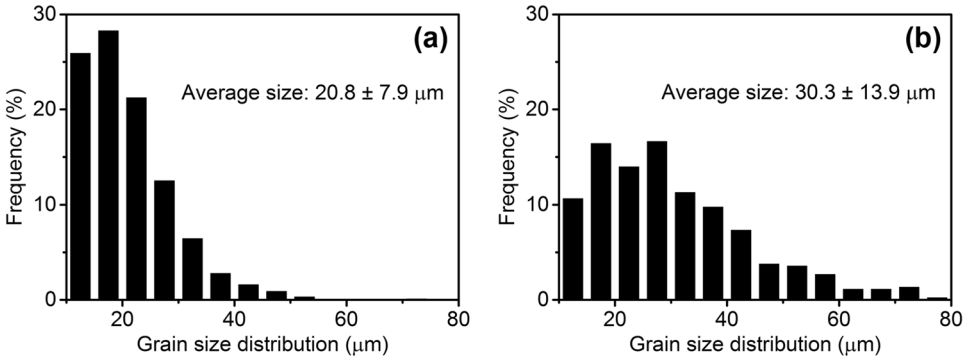

Fig. 4 Grain size distribution histograms of **a** the WC and **b** the FC specimens; those with sizes below 10 μm are discounted so that only bulk grains (rather than plate structures produced by phase transformation) are included

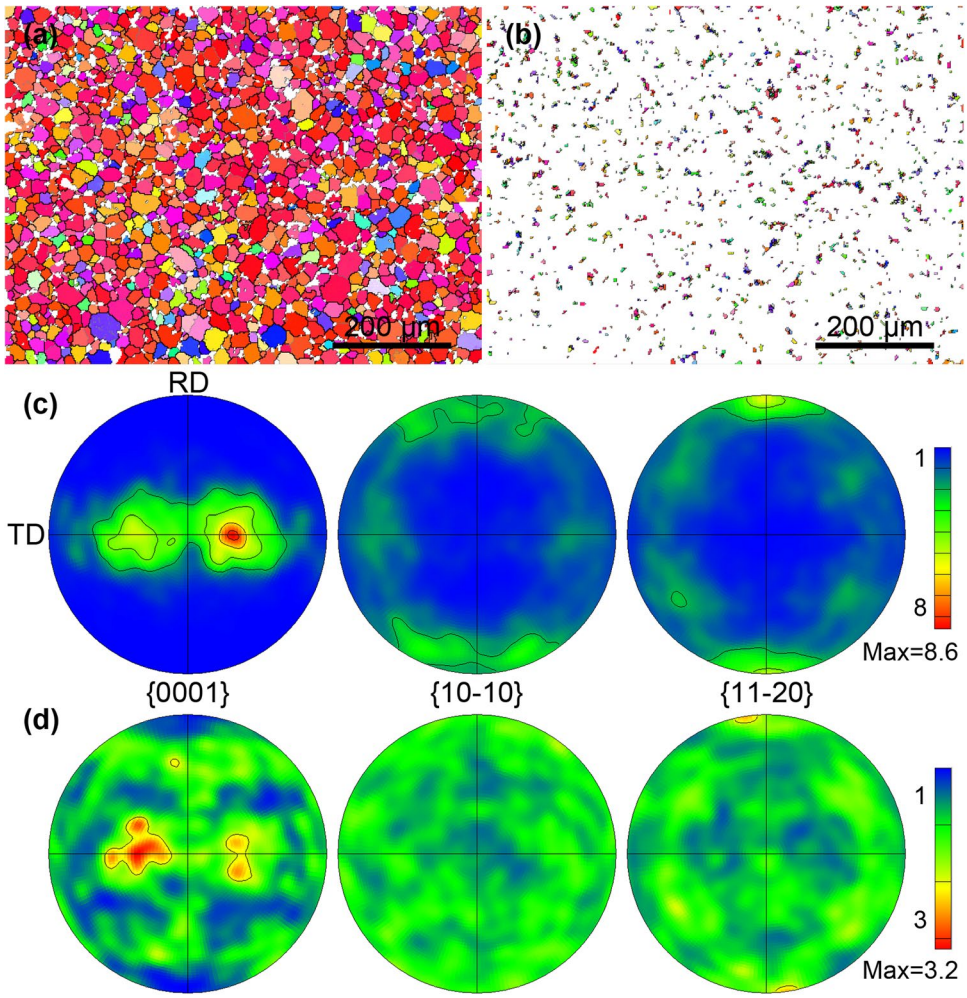

Fig. 5 **a**, **b** Separately present grains with sizes above and below 10 μm in Fig. 3a; **c**, **d** are pole figures corresponding to **a** and **b**, respectively. (Color figure online)

textural features to the bimodal basal texture of the starting material, with a slightly intensified density (8.6 times random). However, the texture of the plate structures is found to be largely randomized with the maximum density of only 3.2 times random (Fig. 5d). This suggests that limited textural changes could occur through growth (coarsening) of the equiaxed grains during annealing at 900 °C. In contrast, martensitic plates induced by the water cooling have scattered orientations, which directly contribute to the globally weakened texture of the WC specimen (Fig. 3).

An elaborate EBSD scanning (at a fine step of 100 nm) for local duplex microstructures in the WC specimen is made and analyzed in Fig. 6. From the band contrast map presented in Fig. 6a, one can see a cluster of plates surrounded by several bulk grains. The bulk grains correspond to grown prior equiaxed α grains while the plates should be

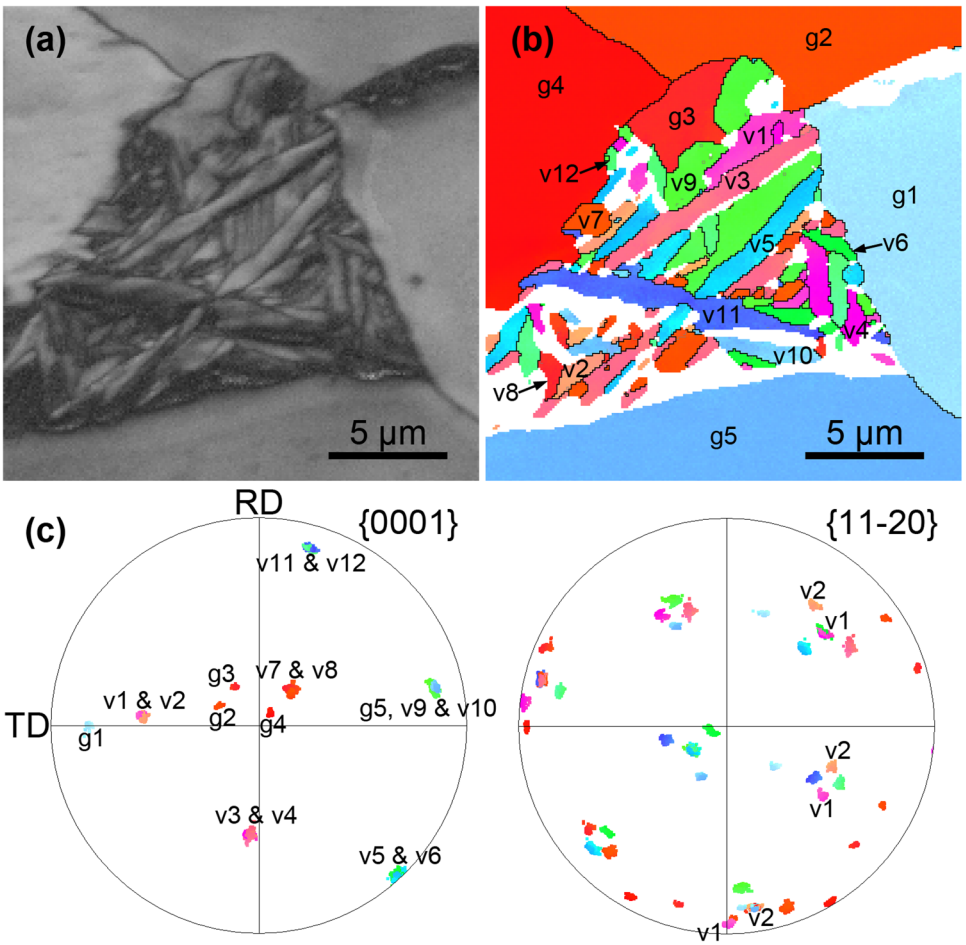

Fig. 6 Local analyses for duplex structures in the WC specimen (step size 0.1 μm): **a** band contrast map, **b** IPF map and **c** pole figures; bulk grains and plate variants are marked by "g#" and "v#" in **b**, **c**, respectively. (Color figure online)

transformed from one or more high-temperature β phases. Furthermore, their orientations are indicated by colors in Fig. 6b and pole figures in Fig. 6c. As labeled by consecutive numbers (g#), five bulk grains with varied orientations are observed. Meanwhile, for the plate structures, twelve different orientations (colors) can be distinguished from Fig. 6b, as marked by v1–v12. This is coincident with the predicted maximum α-variant number from a single β orientation according to the Burgers OR [15]. Also, the OR tells that only five possible misorientations exist between two α variants generated by the same β parent, i.e. 10.5°/<0001>, 60°/<11–20>, 60.8°/~<12–31>, 63.3°/~<44–83>, and 90°/~<12–30> [32]. According to the {0001} pole figure in Fig. 6c, orientations of these plates are found to be grouped into six pairs, with each pair (for instance v1 and v2) sharing the same c-axis. Moreover, the {11–20} pole figure reveals that a-axes of the same pair always deviate ~ 10° from each other. Thus, an orientation relationship of ~ 10°/<0001> is confirmed between them, corresponding to the first Burgers misorientation. After performing similar analyses (not shown here), the other four Burgers misorientations can also be verified between these plates, suggesting that they are α variants transformed from the same β phase.

In regards to the OR between the plates and neighboring bulk grains, Fig. 6c reveals that most of the plates are oriented differently from the bulk grains. The only exception is for v10 and g5, both of which share an exactly identical orientation. A possible explanation is that during heating g5 gives birth to one β orientation, which then acts as the parent of these transformed plates during cooling. As a result, the initial α orientation (g5) is fully inherited by one of the plates (v10) in the location. Nevertheless, the presence of multiple α variants unavoidably leads to greatly scattered orientations, contributing to weakened texture of the WC specimen.

3.3 Variant Selection During β → α Cooling

From the above illustration, a clear effect of cooling rates on the transformation texture is demonstrated for cp-Zr after annealing in the α + β region. Such difference may be understood after considering variant selection behaviors during β → α cooling [11–13]. In earlier studies, α-Zr embryos were found to prefer to nucleate near the parent β boundaries upon slow cooling (allowing sufficient diffusion) [18, 33]. In the case of dual-phase annealing, the embryos tend to maintain

the orientations of pre-existing (untransformed) α phases beside such β boundaries to lower the transformation energy [12]. This means that only a limited number of α variants will be preferably generated by the parent β phase. As a result, due to such strong variant selection, the prior α-Zr texture could be well inherited or even intensified after the phase transformation, like in our FC specimen (Fig. 3d).

As for fast cooling (like water quenching), a large undercooling can be induced, which allows α embryos to nucleate at many sites inside β phases [18, 34]. These α phases often present intersected plate morphologies after growth (for example Fig. 2b). It is clear that orientations of such α embryos formed in β-phase interiors will no longer be affected by any pre-existing α phases. Instead, at most twelve different α orientations are allowed to be generated by a single β orientation according to the Burgers OR [15]. The more α variants are produced, the more scattered orientations can be expected. Interestingly, all the twelve α variants are definitely found to be present in the WC specimen, as exemplified in Fig. 6. This suggests that the rapid cooling in water could facilitate suppression of the α-variant selection. Similar results have also been reported for other rapidly β-quenched Zr alloys in recent work [32, 35]. As a result, a greatly randomized texture will be produced when a large number of such plates are generated by many different β orientations, as verified in Fig. 5b and d. Combined with the slightly changed texture of the bulk grains (Fig. 5a, c), a globally weakened texture is then obtained for the WC specimen (Fig. 3a, c).

4 Conclusions

Specimens cut from a rolled and recrystallized cp-Zr sheet were annealed at 900 °C (corresponding to α + β region) and then subjected to water and furnace cooling. FEG-SEM based ECC imaging and EBSD techniques were utilized to investigate microstructural and textural characteristics of the specimens cooled at different rates, with main conclusions drawn as follows:

1. The WC specimen owns a duplex microstructure consisting of untransformed bulk α grains and twinned martensitic plates; the FC specimen has a uniform microstructure comprised of fully equiaxed grains.
2. After annealing in the α + β region, the prior bimodal basal texture is weakened after rapid cooling in water but strengthened in the case of slow furnace cooling.
3. Water cooling allows various α plates (variants) with scattered orientations to be nucleated inside β phases, contributing to the weakened texture. However, strong variant selection occurs due to preferable nucleation of α phases at β boundaries during furnace cooling, leading to the intensified texture.

Acknowledgements This work was financed by the National Natural Science Foundation of China (Grant Nos. 51401040 and 51601075) and the Fundamental and Cutting-Edge Research Plan of Chongqing (cstc2017jcyjAX0114).

References

1. Z. Duan, H. Yang, Y. Satoh, K. Murakami, S. Kano, Z. Zhao, J. Shen, H. Abe, Current status of materials development of nuclear fuel cladding tubes for light water reactors. Nucl. Eng. Des. **316**, 131–150 (2017)
2. B.X. Zhou, M.Y. Yao, Z.K. Li, X.M. Wang, J. Zhou, C.S. Long, Q. Liu, B.F. Luan, Optimization of N18 zirconium alloy for fuel cladding of water reactors. J. Mater. Sci. Technol. **28**, 606–613 (2012)
3. T.L. Yau, Corrosion of zirconium and its alloys. Shreir's Corros. **3**, 2094–2134 (2010)
4. Z.N. Yang, F.C. Zhang, L. Qu, Z.G. Yan, Y.Y. Xiao, R.P. Liu, X.Y. Zhang, Formation of duplex microstructure in Zr–2.3Nb alloy and its plastic behaviour at various strain rates. Int. J. Plast. **54**, 163–177 (2014)
5. L. Chai, S. Wang, H. Wu, N. Guo, H. Pan, L. Chen, K.L. Murty, B. Song, α → β transformation characteristics revealed by pulsed laser-induced non-equilibrium microstructures in duplex-phase Zr alloy. Sci. China Technol. Sci. **60**, 1255–1262 (2017)
6. E. Tenckhoff, Review of deformation mechanisms, texture, and mechanical anisotropy in zirconium and zirconium base alloys. J. ASTM Int. **2**, 25–50 (2005)
7. L. Chai, B. Luan, D. Xiao, M. Zhang, K.L. Murty, Q. Liu, Microstructural and textural evolution of commercially pure Zr sheet rolled at room and liquid nitrogen temperatures. Mater. Des. **85**, 296–308 (2015)
8. D. Fuloria, N. Kumar, R. Jayaganthan, S.K. Jha, D. Srivastava, An investigation of effect of annealing at different temperatures on microstructures and bulk textures development in deformed Zircaloy-4. Mater. Charact. **129**, 217–233 (2017)
9. K. Murty, I. Charit, Texture development and anisotropic deformation of zircaloys. Prog. Nucl. Energy **48**, 325–359 (2006)
10. B. Luan, S. Gao, L. Chai, X. Li, A. Chapuis, Q. Liu, Compression deformation behavior of Zr–1Sn–0.3Nb alloy with different initial orientations at 650°C. Mater. Des. **52**, 1065–1070 (2013)
11. J. Romero, M. Preuss, J. Quinta da Fonseca, Texture memory and variant selection during phase transformation of a zirconium alloy. Acta Mater. **57**, 5501–5511 (2009)
12. M.R. Daymond, R.A. Holt, S. Cai, P. Mosbrucker, S.C. Vogel, Texture inheritance and variant selection through an hcp–bcc–hcp phase transformation. Acta Mater. **58**, 4053–4066 (2010)
13. M. Sattari, R.A. Holt, M.R. Daymond, Variant selection and transformation texture in zirconium alloy Excel. J. Nucl. Mater. **453**, 120–123 (2014)
14. Y. Ben Ammar, A. Aoufi, M. Darrieulat, Influence of the cooling rate on the texture and the microstructure of Zircaloy-4 studied by means of a Jominy end-quench test. Mater. Sci. Eng. A **556**, 184–193 (2012)
15. W.G. Burgers, On the process of transition of the cubic-body-centered modification into the hexagonal-close-packed modification of zirconium. Physica **1**, 561–586 (1934)

16. H.R. Wenk, I. Lonardelli, D. Williams, Texture changes in the hcp - > bcc - > hcp transformation of zirconium studied in situ by neutron diffraction. Acta Mater. **52**, 1899–1907 (2004)
17. N. Gey, M. Humbert, E. Gautier, J.L. Béchade, Study of the β → α variant selection for a zircaloy-4 rod heated to the β transus in presence or not of an axial tensile stress. J. Nucl. Mater. **328**, 137–145 (2004)
18. R.A. Holt, The beta to alpha phase transformation in zircaloy-4. J. Nucl. Mater. **35**, 322–334 (1970)
19. M. Zhang, F. Zhang, Z. Yang, Y. Li, L. Qu, H. Zhen, Effect of cooling process on the formation of duplex microstructure in Zr–2.3Nb alloy. J Alloys Compd. **651**, 316–321 (2015)
20. Y.H. Jeong, K.S. Rheem, C.S. Choi, Y.S. Kim, Effect of beta heat treatment on microstructure and nodular corrosion of Zircaloy-4. J. Nucl. Sci. Technol. **30**, 154–163 (1993)
21. L. Chai, B. Luan, J. Chen, J. Zhou, Q. Liu, Effect of cooling rate on β → α transformation during quenching of a Zr–0.85Sn–0.4Nb–0.4Fe–0.1Cr–0.05Cu alloy. Sci. China Technol. Sci. **55**, 2960–2964 (2012)
22. L. Chai, B. Luan, B. Chen, H. Yang, Q. Liu, W. Huang, Concurrent inheritance of microstructure and texture after slow β → α cooling of commercially pure Zr. Sci. China Technol. Sci. **59**, 1771–1776 (2016)
23. X.H. Zheng, H.W. Zhang, Experimental determination of deformation induced lattice rotation by EBSD technique for slip system analysis. J. Mater. Sci. Technol. **33**, 90–98 (2017)
24. V. Randle, Electron backscatter diffraction: strategies for reliable data acquisition and processing. Mater. Charact. **60**, 913–922 (2009)
25. L. Chai, H. Wu, S. Wang, K. Chen, T. Wang, J. Xia, Characterization of microstructure and hardness of a Zr-2.5Nb alloy surface-treated by pulsed laser. Mater. Chem. Phys. **198**, 303–309 (2017)
26. H.L. Yang, Y. Matsukawa, S. Kano, Z.G. Duan, K. Murakami, H. Abe, Investigation on microstructural evolution and hardening mechanism in dilute ZrNb binary alloys. J. Nucl. Mater. **481**, 117–124 (2016)
27. Y.I. Jung, M.H. Lee, H.G. Kim, J.Y. Park, Y.H. Jeong, Behavior of a recrystallization in HANA-4 and HANA-6 zirconium-based alloys. J. Alloys Compd. **479**, 423–426 (2009)
28. L.Y. Chen, Q.F. Zeng, J.X. Li, J.Q. Lu, Y. Zhang, L.C. Zhang, X.J. Qin, W.J. Lu, L.F. Zhang, L.Q. Wang, D. Zhang, Effect of microstructure on corrosion behavior of a Zr–Sn–Nb–Fe–Cu–O alloy. Mater. Des. **92**, 888–896 (2016)
29. Z.N. Yang, Y.Y. Xiao, F.C. Zhang, Z.G. Yan, Effect of cold rolling on microstructure and mechanical properties of pure Zr. Mater. Sci. Eng. A **556**, 728–733 (2012)
30. H. Yang, S. Kano, Y. Matsukawa, Y. Li, J. Shen, F. Li, Z. Zhao, Y. Satoh, H. Abe, Effect of molybdenum on microstructures in Zr-1.2 Nb alloys after β-quenching and subsequently 873 K annealing. Mater. Des. **104**, 355–364 (2016)
31. H.G. Kim, J.H. Baek, S.D. Kim, Y.H. Jeong, Microstructure and corrosion characteristics of Zr–1.5Nb–0.4Sn–0.2Fe–0.1Cr alloy with a beta-annealing. J. Nucl. Mater. **372**, 304–311 (2008)
32. L. Chai, B. Chen, Z. Zhou, K.L. Murty, Y. Ma, W. Huang, A special twin relationship or a common Burgers misorientation between α plates after β quenching in Zr alloy? Mater. Charact. **104**, 61–65 (2015)
33. J. Crepin, T. Bretheau, D. Caldemaison, Plastic-deformation mechanisms of beta-treated zirconium. Acta Metall. Mater. **43**, 3709–3719 (1995)
34. D.O. Northwood, D.T. Lim, Phase-transformations in zirconium and its alloys. Can. Metall. Q. **18**, 441–467 (1979)
35. L. Chai, B. Luan, M. Zhang, K.L. Murty, Q. Liu, Experimental observation of 12 α variants inherited from one β grain in a Zr alloy. J. Nucl. Mater. **440**, 377–381 (2013)